

Liquid–Liquid Phase Equilibria in Porous Materials[†]

M. Sliwinska-Bartkowiak,[‡] S. L. Sowers,[§] and K. E. Gubbins^{*,§}

Instytut Fizyki, Uniwersytet im Adama Mickiewicza, ul. Grunwaldzka 6, 60-780 Poznan, Poland, and School of Chemical Engineering, Cornell University, Ithaca, New York 14853-5201

Received January 2, 1996. In Final Form: June 10, 1996[⊗]

Theoretical and experimental results are presented for the effect of confinement on liquid–liquid phase equilibria for binary mixtures. Density functional theory calculations for a symmetric Lennard-Jones mixture in pores show the following qualitative features: a reduction in the critical mixing temperature, and a shift in the coexistence curve toward the component 1-rich side of the phase diagram when molecules of component 1 are more strongly attracted to the walls. These effects become more pronounced for smaller pores. Experimental results are presented for nitrobenzene/*n*-hexane mixtures in a controlled pore glass having pores of mean width 100 nm. Results for the liquid–liquid coexistence in the pores are obtained using nonlinear dielectric effect (NDE) and light transmission measurements. The effect of confinement is to produce a lowering of the critical mixing temperature by 0.05 ± 0.02 K and a shift in the critical mixing composition toward the nitrobenzene-rich side of the diagram by 0.04 ± 0.01 in mole fraction. Measurements near the pore critical point show that the NDE tends to a finite value at the critical point, apparently due to the constraint on the growth of the correlation length due to the pore walls.

1. Introduction

The most well-known and widely studied phase transitions in pores have been capillary condensation, layering transitions, and wetting. Studies over the last decade using density functional theory,¹ molecular simulation,¹ and experiments (e.g., ref 2) on well-characterized porous materials have provided considerable insight into the nature of these transitions. Other important transitions that are much less studied include melting, solid–solid transitions, solubility phenomena, and liquid–liquid transitions.

Liquid–liquid transitions are of interest in connection with oil recovery, lubrication, coating technology, and pollution control. The effect of confinement on the solubility of dilute solutes is largely unknown at present but is of great importance in understanding the dispersion of pollutants in soils, in removing trace pollutants from water, where concentrations are usually less than 10^{-3} M, and in lubrication.

In this paper we present a theoretical and experimental study of confinement effects on liquid–liquid phase transitions in well-characterized porous materials. Questions that are ultimately of interest to us include the following. What is the influence of confinement on the liquid–liquid coexistence curve and on the critical mixing point? How is this affected by pore size and other pore characteristics (shape, material), nature of solute and solvent, and state conditions? How do these effects differ for symmetric and unsymmetric mixtures? Can solubility

be controlled by suitably tailoring the state condition, pore size, pore shape, or material? The work reported here is an initial step toward answering some of these questions. We report density functional theory calculations for liquid–liquid phase separation in pores using a simple, symmetric Lennard-Jones model fluid; these calculations serve to show some of the main qualitative effects of confinement and fluid–wall interactions. We also report what we believe are the first experimental results for such phase equilibria in well-characterized materials (a controlled pore glass) having a nearly monodisperse pore size. The experimental studies also provide insight into finite size effects near the critical point.

There have been few experimental studies of liquid–liquid transitions reported for monodisperse pores. Christenson and Blom³ made solvation force measurements which suggest they may have observed liquid–liquid phase separation in a mixture of water and octomethylcyclotetrasiloxane (OMCTS). However, their results did not produce the coexistence curve for liquid–liquid equilibrium (LLE) in the pores. LLE has also been studied in thin films of polymer blends,^{4–6} and it has been found that, in addition to a shift in the coexistence curve to different compositions, the LL critical temperature is shifted. For such polymer blends, shifts in the coexistence curve are found even for pores as large as $1 \mu\text{m}$ (1000 nm). So far these experimental studies of LLE for both simple and polymeric fluids are not sufficiently advanced to provide any simple physical picture of the effects of confinement on LLE or solubility, in contrast to the situation for capillary condensation and melting. In addition to this work on well-characterized pores, there is a body of experimental and theoretical work on LL phase separation near the critical mixing point for more random pore structures (see ref 7 and references therein); much of the interest in these studies is the possibility of random field Ising critical behavior due to the interconnected pore network.

[†] Presented at the Second International Symposium on Effects of Surface Heterogeneity in Adsorption and Catalysis on Solids, held in Poland/Slovakia, September 4–10, 1995.

[‡] Uniwersytet im Adama Mickiewicza.

[§] Cornell University.

[⊗] Abstract published in *Advance ACS Abstracts*, September 15, 1996.

(1) The literature on DFT and simulation studies of phase transitions in pores is too extensive to review here. An overview of some typical recent work can be found in the proceedings of the Fundamentals of Adsorption Conferences, held every three years. See *Proceedings of the Fourth International Conference on Fundamentals of Adsorption*; Suzuki, M., Ed.; Engineering Foundation: New York, 1993. *Proceedings of the Fifth International Conference on Fundamentals of Adsorption*; LeVan, M. D., Ed.; in press.

(2) Findenegg, G. H.; Gross, S.; Michalski, T. *Characterization of Porous Solids III*; Rouquerol, J., Ed.; Elsevier: Amsterdam, 1994; p 71. Thommes, M.; Findenegg, G. H. *Langmuir* **1994**, *10*, 4270.

(3) Christenson, H. K.; Blom, C. E. *J. Chem. Phys.* **1987**, *71*, 192.

(4) Reich, S.; Cohen, Y. *J. Polym. Sci.* **1981**, *19*, 1255.

(5) Budkowski, A.; Steiner, U.; Klein, J. *J. Chem. Phys.* **1992**, *97*, 5229.

(6) Bruder, F.; Brenn, R. *Phys. Rev. Lett.* **1992**, *69*, 624.

(7) Lin, M. Y.; Sinha, S. K.; Drake, J. M.; Wu, X.-I.; Thiyagarajan, P.; Stanley, H. B. *Phys. Rev. Lett.* **1994**, *72*, 2207. Monette, L.; Liu, A. J.; Grest, G. S. *Phys. Rev. A* **1992**, *46*, 7664.

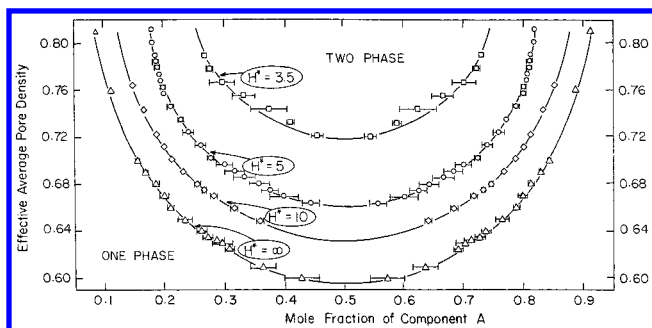


Figure 1. Liquid–liquid equilibrium coexistence curves for a symmetrical LJ mixture with parameters characteristic of methane and with unlike pair parameter $\xi_{12} = 0.65$, in slit carbon pores (with 10, 4, 3 walls) of width H ($H^* = H/\sigma$) at $T^* = 1.2$. The pressure of the bulk fluid was varied to produce various average densities in the pore. Results are from Gibbs Ensemble Monte Carlo simulations, based on results of Gózdź et al.⁸

Two molecular simulation studies of liquid–liquid equilibria in pores have been reported recently for a simple Lennard-Jones symmetrical mixture.^{8,9} In both studies the fluid mixture has like pair interactions, u_{11} and u_{22} , that are identical ($\epsilon_{11} = \epsilon_{22}$, $\sigma_{11} = \sigma_{22}$), while the attractive part of the unlike pair interaction u_{12} is considerably weaker than the geometric mean ($\epsilon_{12} = k(\epsilon_{11}\epsilon_{22})^{1/2}$, $\sigma_{12} = \sigma_{11} = \sigma_{22}$, where k is much less than unity). The weak unlike pair interaction leads to liquid–liquid immiscibility in the bulk mixture, and the symmetry of the potential produces a liquid–liquid coexistence curve that is symmetrical about $x_1 = 0.5$, a homogeneous positive azeotrope at $x_1 = 0.5$ for higher pressures, and a heterogeneous azeotrope at low pressures.^{9–12} We shall refer to this model mixture as the *symmetrical LJ mixture*. In these studies of the confined fluid, the two components had the same interaction potential with the pore walls, and the pores were of slit shape; thus the mixture was also symmetrical with respect to components 1 and 2 in the pore, and the results show the effects of pure confinement. The results from these two studies were very similar, and typical coexistence curves are shown in Figure 1. The main qualitative conclusions are that confinement leads to (a) a decreased region of immiscibility (i.e., selective adsorption of the dilute component), and (b) a lowering of the critical solution temperature. The decreased immiscibility range is at first sight surprising, since the two components experience the same fluid–wall interaction. It arises because the effect of the weak unlike pair interaction is reduced as a result of the lower dimensionality associated with decreased pore size.

In a related study, Kumar et al.¹³ have reported Gibbs Ensemble Monte Carlo simulations for a symmetric mixture of LJ chain molecules (like pair interactions the same, weak unlike molecule pair interactions). The LL coexistence curves found for this symmetric chain molecule mixture were qualitatively similar to those found for the symmetric LJ mixture and shown in Figure 1 (increased solubility of the dilute component, and a lowering of T_c).

Our paper is arranged as follows. In section 2 we outline the density functional theory and model used. Theoretical

results are given in section 3, and the experimental method and results are given in Sections 4 and 5, respectively.

2. Theory

For large pores it is possible to derive thermodynamic relationships between the confinement effect and the various surface tensions involved.^{14–16} The equations for liquid–liquid separation in confined mixtures have been given by Evans and Marini Bettolo Marconi.¹⁶ If μ_2^b and μ_2^p are the chemical potentials for component 2 for the coexisting phases α and β in the bulk mixture and in the pore, respectively, and if the α phase is the one rich in 2, then

$$\mu_2^b - \mu_2^p = \frac{2\gamma_{\alpha\beta} \cos \theta}{r_p B \rho_{1,\alpha}} \quad (1)$$

where $\gamma_{\alpha\beta}$ is the interfacial tension between the two fluid phases, θ is the contact angle between the $\alpha\beta$ meniscus and the wall, r_p is the pore radius, $\rho_{1,\alpha}$ is the number density of the α phase at chemical potential μ_2 , and $B = (x_2^b/x_1^b)_\alpha - (x_2^b/x_1^b)_\beta$. If the contact angle $\theta < \pi/2$ phase separation in the pore will occur for $\mu_2^p < \mu_2^b$, i.e., at smaller mole fractions x_2 ; this will occur when the wall favors the α phase. The reverse will hold when $\theta > \pi/2$.

Equation 1 will break down for small pores. Molecular simulations^{17,18} have shown that for simple fluids like nitrogen, Kelvin's equation (the analog of (1) for capillary condensation) fails for pore diameters below about 7.5 nm and is in very serious error for micropores (diameters below 2 nm). In this work, therefore, we use the Kierlik–Rosinberg–Rosenfeld¹⁹ form of density functional theory for our calculations.

2.1. Model System. The intermolecular fluid interactions are modeled using the truncated Lennard-Jones (LJ) potential

$$\phi_{ij}(r_{ij}) = \begin{cases} 4\epsilon_{ij} \left[\left(\frac{\sigma_{ij}}{r_{ij}} \right)^{12} - \left(\frac{\sigma_{ij}}{r_{ij}} \right)^6 \right] & r_{ij} < R_c \\ 0 & r_{ij} > R_c \end{cases} \quad (2)$$

where σ_{ij} and ϵ_{ij} are the LJ size and energy parameters, R_c is the cutoff radius, and r_{ij} is the interparticle distance. R_c was set equal to 15σ , where σ is the fluid–fluid interaction parameter. Calculations were performed using the LJ sphere model for a symmetric fluid, where $\sigma_{11} = \sigma_{12} = \sigma_{22} = \sigma$, $\epsilon_{11} = \epsilon_{22} = \epsilon$, and $\epsilon_{12} = k\epsilon$, where k is much less than unity. The departure of the parameter k from unity is a measure of the nonideality of the mixture. For this work we chose $k = 0.8$. The phase diagram is of class II in the classification scheme of van Konynenburg and Scott.²⁰ For the fluid, the LJ size and energy parameters are chosen to be those of argon: $\sigma = 3.405 \text{ \AA}$, $\epsilon/k_B = 119.8 \text{ K}$.

The sorbent is modeled as a graphitic slit pore, with the interactions between the fluid particles and the flat

(14) Epstein, P. S. *Textbook of Thermodynamics*; Wiley: New York, 1954; Chapter 12.

(15) Defay, R.; Prigogine, I. *Surface Tension and Adsorption*; Longman's: London, 1966; Chapter 15.

(16) Evans, R.; Marini Bettolo Marconi, U. *J. Chem. Phys.* **1987**, *86*, 7138.

(17) Lastoskie, C.; Gubbins, K. E.; Quirke, N. *Characterization of Porous Solids III*; Rouquerol, J., Ed.; Elsevier: Amsterdam, 1994; p 51.

(18) Lastoskie, C.; Gubbins, K. E.; Quirke, N. *Langmuir* **1993**, *9*, 2693.

(19) Kierlik, E.; Rosinberg, M. *Phys. Rev. A* **1990**, *42*, 3382; *Phys. Rev. A* **1991**, *44*, 5025. This theory has recently been shown to be equivalent to the earlier DFT of Rosenfeld (Rosenfeld, Y. *Phys. Rev. Lett.* **1989**, *63*, 980). See Phan, S.; Kierlik, E.; Rosinberg, M. L.; Bildstein B.; Kahl, G. *Phys. Rev. E* **1993**, *48*, 618.

(20) van Konynenburg, P. H.; Scott, R. *Philos. Trans.* **1980**, *298*, 495.

(8) Gózdź, W. T.; Gubbins, K. E.; Panagiotopoulos, A. Z. *Mol. Phys.* **1995**, *84*, 825.

(9) Kierlik, E.; Fan, Y.; Monson, P. A.; Rosinberg, M. L. *J. Chem. Phys.* **1995**, *102*, 3712.

(10) Panagiotopoulos, A. Z. *Int. J. Thermophys.* **1989**, *10*, 447.

(11) Stapleton, M. R.; Panagiotopoulos, A. Z. *J. Chem. Phys.* **1990**, *92*, 1285.

(12) Fan, Y.; Finn, J. E.; Monson, P. A. *J. Chem. Phys.* **1993**, *99*, 8238.

(13) Kumar, S. K.; Tang, H.; Szleifer, I. *Mol. Phys.* **1994**, *81*, 867.

graphitic surface of the pore wall taken as the 10–4–3 potential of Steele²¹

$$\phi_{\text{sf}} = A \left[\frac{2}{5} \left(\frac{\sigma_{\text{sf}}}{z} \right)^{10} - \left(\frac{\sigma_{\text{sf}}}{z} \right)^4 - \left(\frac{\sigma_{\text{sf}}^4}{3\Delta(z + 0.61\Delta)^3} \right) \right] \quad (3)$$

where $A = 2\pi\rho_s\epsilon_{\text{sf}}\sigma_{\text{sf}}^2\Delta$, ρ_s is the solid density, ϵ_{sf} and σ_{sf} are the parameters for the solid–fluid interactions, calculated using the Lorentz–Berthelot rules, and Δ is the distance between the graphitic planes of LJ atoms. The values for the graphitic parameters are²¹ $\Delta = 0.335$ nm, $\rho_s = 114$ nm⁻², $\sigma_{\text{ss}} = 0.340$ nm, and $\epsilon_{\text{ss}}/k_b = 28.0$ K. The solid–fluid energy parameters are chosen so that the ratios of the parameters for component 1 to component 2 are greater than or equal to unity,

$$\epsilon_{\text{sf}2} = (\epsilon_{\text{ss}}\epsilon)^{1/2}, \quad \epsilon_{\text{sf}1}/\epsilon_{\text{sf}2} \geq 1.0 \quad (4)$$

For ratios greater than unity, component 1 is more strongly attracted to the pore wall. This leads to a shift in the phase diagram for the confined system from its symmetry about $x_1 = 0.5$ in the bulk.

2.2. Density Functional Theory. We use the Rosenfeld–Kierlik–Rosinberg version of DFT¹⁹ in this work. The grand potential functional for the system is given quite generally as

$$\Omega[\{\rho_{ij}\}] = F[\{\rho_{ij}\}] - \sum_i \int d\mathbf{r} \rho_i(\mathbf{r}) [\mu_i - \phi_i^{\text{ext}}(\mathbf{r})] \quad (5)$$

where F is the intrinsic Helmholtz free energy functional, μ_i is the chemical potential of component i , and $\phi_i^{\text{ext}}(\mathbf{r})$ is the varying external potential.

The contributions to F are then separated into hard-sphere reference fluid, $F_{\text{hs}}[\{\rho_{ij}\}]$, and attractive, $\Delta F_{\text{attr}}[\{\rho_{ij}\}]$, components

$$F[\{\rho_{ij}\}] = F_{\text{hs}}[\{\rho_{ij}\}] + \Delta F_{\text{attr}}[\{\rho_{ij}\}] \quad (6)$$

$\Delta F_{\text{attr}}[\{\rho_{ij}\}]$ is then represented in the mean field approximation as

$$\Delta F_{\text{attr}}[\{\rho_{ij}\}] = \frac{1}{2} \sum_{ij} \int \int d\mathbf{r} d\mathbf{r}' \rho_i(\mathbf{r}) \rho_j(\mathbf{r}') \phi_{ij}^{\text{attr}}(|\mathbf{r} - \mathbf{r}'|) \quad (7)$$

where $\rho_i(\mathbf{r})$ is the number density of component i at position \mathbf{r} and ϕ_{ij}^{attr} is the attractive part of the fluid–fluid potential, given by the Weeks–Chandler–Andersen²² division of the LJ potential. The hard sphere diameter is calculated using the Barker–Henderson expression

$$d = \int_0^{r^*} [1 - \exp(-u_0(r)/kT)] dr \quad (8)$$

where $u_0(r)$ is the repulsive part of the potential, as defined in the WCA theory. The hard-sphere term F_{hs} is further split into ideal gas and excess components,

$$F_{\text{hs}}[\{\rho_{ij}\}] = F^{\text{id}}[\{\rho_{ij}\}] + F_{\text{hs}}^{\text{ex}}[\{\rho_{ij}\}] \quad (9)$$

where F^{id} is the (local) ideal gas contribution, and the excess part is given by^{23,24}

$$F_{\text{hs}}^{\text{ex}}[\{\rho_{ij}\}] = kT \int d\mathbf{r} \psi [n_\alpha(\mathbf{r})] \quad (10)$$

where $kT\psi$ is the excess part of the Helmholtz free energy density of the uniform hard-sphere fluid for a smoothed density $n_\alpha(\mathbf{r})$, defined as

$$n_\alpha(\mathbf{r}) = \sum_i \int d\mathbf{r}' \rho_i(\mathbf{r}') \omega_i^{(\alpha)}(|\mathbf{r} - \mathbf{r}'|) \quad (11)$$

where $\omega_i^{(\alpha)}$ ($\alpha = 1-4$) are the weighting functions. ψ is taken from the scaled particle theory or the Percus–Yevick compressibility equation of state for a uniform hard-sphere mixture.²⁵ The four weight functions $\omega_i^{(\alpha)}$ are scalars that are related to the Heaviside step function and its derivatives. They are independent of density, which is the principal difference from other nonlocal approximations:

$$\omega_i^{(3)}(\mathbf{r}) = \Theta(R_i - r)$$

$$\omega_i^{(2)}(\mathbf{r}) = \delta(R_i - r)$$

$$\omega_i^{(1)}(\mathbf{r}) = -(1/8) \delta'(R_i - r)$$

$$\omega_i^{(0)}(\mathbf{r}) = -(1/8) \delta'(R_i - r) + (1/2\pi R_i) \delta''(R_i - r) \quad (12)$$

The equilibrium density profile is found by solving

$$\frac{\delta\Omega[\{\rho_{ij}\}]}{\delta\rho_i(r)} = 0 \quad \text{at} \quad \rho_i = \rho_{i,\text{eq}} \quad (13)$$

The equation of state of the homogeneous fluid can be obtained from the generic free energy functional. The pressure of the homogeneous fluid is composed of a hard-sphere pressure, P_{hs} , and a mean field attractive contribution

$$P = P_{\text{hs}} + 2\pi\rho^2 \sum_{ij} x_i x_j \int \phi_{ij}^{\text{attr}}(r) r^2 dr \quad (14)$$

The chemical potential of the fluid is

$$\mu_i = \mu_i^{\text{hs}} + 4\pi\rho \sum_j x_j \int \phi_{ij}^{\text{attr}}(r) r^2 dr \quad (15)$$

where μ_i^{hs} is the hard sphere contribution. The mean field equation of state was used to produce the bulk phase diagram, which is symmetric about $x_1 = 0.5$. Due to the symmetry of the system, at phase coexistence the chemical potentials μ_i in the two phases α and β are equal for both components

$$\mu_i^\alpha = \mu_i^\beta \quad (16)$$

Bulk phase diagrams for various values of k are shown in Figure 2. When the two components have the same solid–fluid energy parameter, the symmetry holds as well for the confined system. For a ratio of solid–fluid parameters of the two components which is not equal to 1, the symmetry of the coexistence curve about $x_1 = 0.5$ is lost. Coexistence is found when the grand free energy, or, alternatively, the surface tension γ , and the chemical

(21) Steele, W. A. *Surf. Sci.* **1973**, *36*, 317. Steele, W. A. *The Interaction of Gases With Solid Surfaces*; Pergman: Oxford, 1974.

(22) Weeks, J. D.; Chandler, D.; Andersen, H. L. *J. Chem. Phys.* **1971**, *54*, 5237.

(23) Percus, J. J. *Stat. Phys.* **1988**, *52*, 1157.

(24) Rosenfeld, Y. *J. Chem. Phys.* **1990**, *93*, 4305.

(25) Reiss, H.; Frisch, H.; Lebowitz, J. L. *J. Chem. Phys.* **1959**, *31*, 369. Helfand, E.; Frisch, H.; Lebowitz, J. L. *J. Chem. Phys.* **1961**, *34*, 1037.

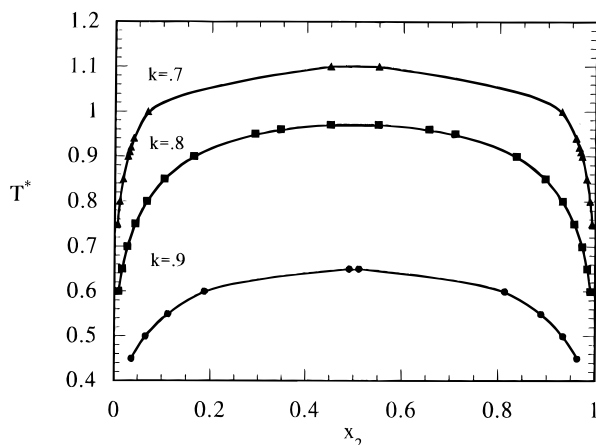


Figure 2. Coexistence curves for the bulk symmetric LJ mixture for $P^* = 0.1$ and various values of k .

Table 1. Conditions for Bulk Liquid/Liquid Phase Coexistence from the Mean Field Equation of State for $P^* = 0.1$ and $k = 0.8$

T^*	ρ^*_{bulk}	x_1	μ^*
0.600	0.9132	0.9906	-4.880
0.650	0.8798	0.9834	-4.714
0.700	0.8465	0.9725	-4.572
0.750	0.8127	0.9563	-4.450
0.775	0.7955	0.9455	-4.398
0.800	0.7778	0.9323	-4.351
0.825	0.7595	0.9161	-4.309
0.850	0.7405	0.8959	-4.272
0.875	0.7204	0.8701	-4.241
0.900	0.6989	0.8358	-4.216
0.950	0.6481	0.7075	-4.185
0.975	0.6181	0.5097	-4.059

potential for each component in both phases are equal

$$\mu_1^\alpha = \mu_1^\beta; \quad \mu_2^\alpha = \mu_2^\beta; \quad \Omega^\alpha = \Omega^\beta \quad (17)$$

where Ω is the minimized grand free energy functional. The surface tension is defined as

$$\gamma = \frac{\Omega + PV}{2A} \quad (18)$$

where P is the pressure, V is the volume, and A is the surface area.

The following dimensionless quantities are used in the calculations: pore width, $H^* = H/\sigma$; temperature, $T^* = kT/\epsilon$; pressure, $P^* = P\sigma^3/\epsilon$; density, $\rho^* = \rho\sigma^3$; chemical potential, $\mu^* = \mu/\epsilon$; and Gibbs adsorption excess, $G_i^* = G_i\sigma^2$.

3. Theoretical Results

Calculations were performed for the symmetric LJ mixture for $P^* = 0.1$ and $k = 0.8$. The conditions for phase coexistence in the bulk mixture are listed in Table 1; $\mu^* = \mu/\epsilon$, where μ is the total chemical potential.

The effect of pore width on the phase diagrams for liquid–liquid equilibrium of the confined fluid for the parameter ratio $\epsilon_{\text{sf1}}/\epsilon_{\text{sf2}} = 1.2$ is shown in Figures 3 and 4. The coexistence curve for the bulk fluid and two reduced pore widths, $H^* = 10.0$ and 20.558 (7 nm), is shown in Figure 3. Confinement causes the region of miscibility to be decreased, and the critical mixing temperature is lowered. The stronger fluid–wall attraction for component 1 leads to a shift in the coexistence curve toward the component 1-rich side. As the pore width is decreased, the selectivity for component 1 increases, and the envelope of miscibility is further decreased. These effects can be seen more clearly in Figure 4, which shows an enlarged

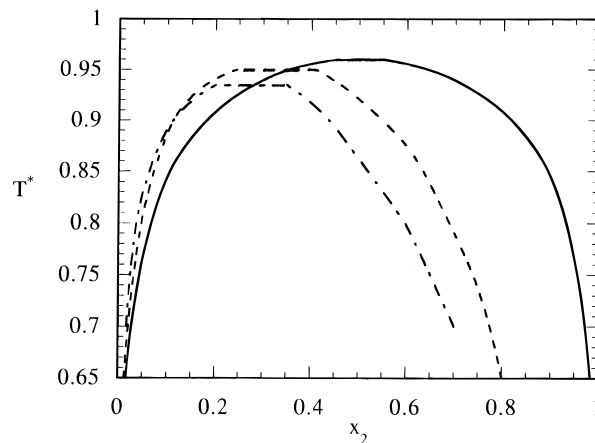


Figure 3. Liquid–liquid phase diagrams for the bulk and confined symmetric LJ mixture for $k = 0.8$, $P^* = 0.1$, $\epsilon_{\text{sf1}}/\epsilon_{\text{sf2}} = 1.2$. The bulk system (solid line) and two pore widths, $H^* = 10.0$ (dotted-dashed line) and 20.558 ($H = 7.0$ nm, dashed line), are shown.

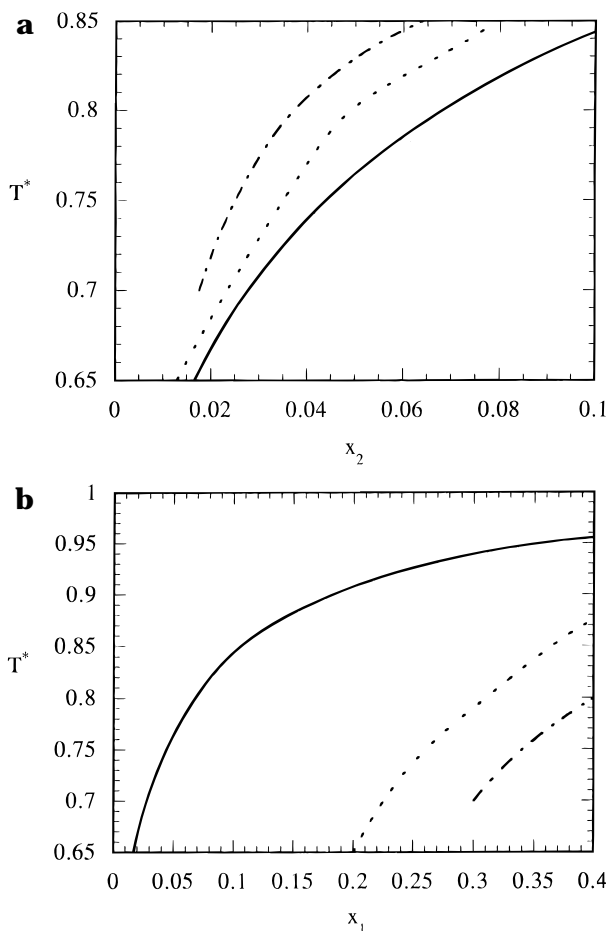
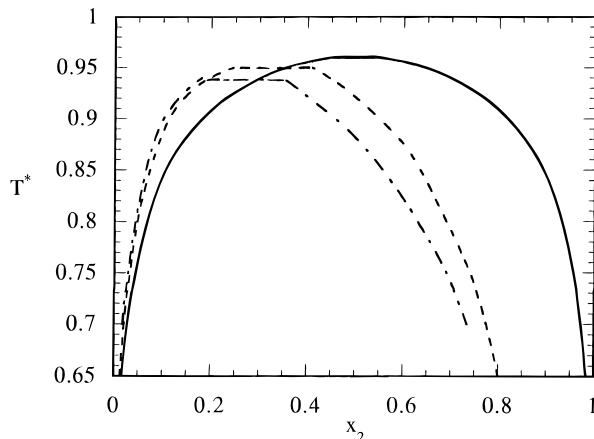


Figure 4. Effect of confinement on solubility of the dilute component for the system of Figure 3: (a) solubility of component 2 in the component 1-rich phase; (b) solubility of component 1 in the component 2-rich phase. Key as in Figure 3.

view of the solubilities of the dilute component in the component 1-rich and component 2-rich phases. The confinement is seen to lead to a substantial decrease in solubility of component 2 in the component 1-rich phase (by 25–50% in the case of the smaller pore). There is a corresponding and much larger increase in solubility of component 1 in the component 2-rich phase (by as much as a factor of 16 at the lower temperatures shown in Figure 4b). The critical temperatures and compositions for these systems are listed in Table 2.

Table 2. Critical Temperatures and Compositions of the Symmetric LJ Mixture for Various Pore Widths and Ratios of Solid–Fluid Interactions of the Two Components

	T_c^*	$\chi_{2,c}$
bulk symmetric fluid	0.975	0.5000
$H^* = 10.0$, $\epsilon_{sf1}/\epsilon_{sf2} = 1.2$	0.935	0.2750
$H^* = 20.558$, $\epsilon_{sf1}/\epsilon_{sf2} = 1.2$	0.950	0.3275
$H^* = 20.558$, $\epsilon_{sf1}/\epsilon_{sf2} = 1.5$	0.940	0.2625

**Figure 5.** Liquid–liquid phase diagrams for the bulk and confined symmetric LJ mixture for $k = 0.8$, $P^* = 0.1$, $H^* = 20.588$. The bulk system (solid line) and two $\epsilon_{sf1}/\epsilon_{sf2}$ ratios, 1.2 (dashed line) and 1.5 (dash-dotted line), are shown.

The effect of the relative strengths of attraction to the pore walls of component 1 to component 2 on the phase equilibria is shown in Figures 5 and 6. The phase diagrams for the bulk fluid and the confined fluid with two ratios of the solid–fluid parameters $\epsilon_{sf1}/\epsilon_{sf2}$ are shown in Figure 5. The effect of increasing this ratio is (a) to decrease the range of miscibility, (b) to further lower the critical mixing temperature, and (c) to further shift the coexistence curve toward the component 1-rich side of the phase diagram. The solubilities of the dilute component in the two phases are shown in Figure 6. Increasing the ratio $\epsilon_{sf1}/\epsilon_{sf2}$ causes the solubility of component 2 in the component 1-rich phase to decrease, while the solubility of component 1 in the component 2-rich phase is increased. The critical temperatures and compositions for the systems studied are listed in Table 2.

4. Experimental Method

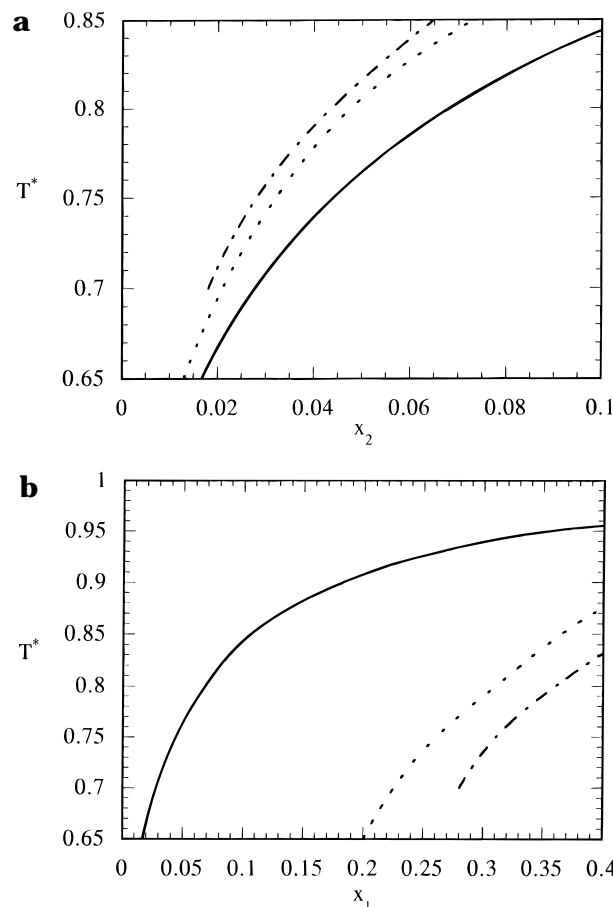
Two experimental methods were used to determine the phase transition temperature and to describe the phase transition character: nonlinear dielectric effect (NDE) and light transmission measurements. Since these methods have been described in detail elsewhere,^{26,27} we give only a brief description here. In both experiments, measurements were made along a path of constant bulk composition, starting at a temperature in the one phase region above the liquid–liquid coexistence line. The temperature was then reduced until the phase transition was observed. This was repeated at different bulk compositions to define the liquid–liquid coexistence curve (T vs x_2 , where component 2 is nitrobenzene).

The NDE is defined as the change in the medium permittivity ϵ in a strong external electric field, E

$$\frac{\Delta\epsilon}{E^2} = \frac{\epsilon^E - \epsilon^0}{E^2} \quad (19)$$

(26) Sliwiska-Bartkowiak, M.; Szurkowski, B.; Hilczer, T. *Chem. Phys. Lett.* **1984**, *94*, 609.

(27) Sikorski, R.; Sliwiska-Bartkowiak, M. *Acta Phys. Polon.*, in press.

**Figure 6.** Effect of confinement on solubility of the dilute component for the system of Figure 5: (a) solubility of component 2 in the component 1-rich phase; (b) solubility of component 1 in the component 2-rich phase. Key as in Figure 5.

where ϵ^E is the permittivity in the electric field E and ϵ^0 is the permittivity in the absence of the field. The NDE is sensitive to the fluid inhomogeneities in the vicinity of the critical point and exhibits an anomalous increase related to the density fluctuation in the medium.^{28–31} The temperature dependence of the NDE, when approaching the critical point along the critical composition line, is described by the following formula^{32–34}

$$\left(\frac{\Delta\epsilon}{E^2}\right)_c \approx \left(\frac{\Delta\epsilon}{E^2}\right) - \left(\frac{\Delta\epsilon}{E^2}\right)_b \approx At^{-\phi} \quad (20)$$

where $(\Delta\epsilon/E^2)_b$ is the background effect, measured at high temperatures and interpolated in the vicinity of the critical temperature,^{35,36} $t = (T - T_c)/T_c$, A is the amplitude, and ϕ is the critical exponent. The ability of eq 20 to describe the data was examined for both the bulk mixture and the mixture confined in controlled pore glass. The permittivity was measured by the pulse method. The measuring capacitor and the measurement method were described in ref 26. The experiments were carried out for both the bulk mixtures and mixtures in controlled pore glass at temperatures ranging from 285 to 305 K ($\pm 10^{-2}$ K).

Light transmission measurements were used to determine the temperature of the phase separation in the mixtures, i.e. the temperature at which a strong turbidity of the system is observed. The experimental setup and the measurement method have been described in ref 27. The vessel containing the liquid was

(28) Piekara, A. *Phys. Rev.* **1932**, *42*, 488.

(29) Zboinski, K. *Chem. Phys. Lett.* **1976**, *39*, 336.

(30) Malecki, J.; Ziolo, J. *Chem. Phys.* **1978**, *35*, 187.

(31) Rzoska, S. J.; Chrapec, J. *Phase Trans.* **1989**, *15*, 1.

(32) Oxtoby, D. W.; Metiu, H. *Phys. Rev. Lett.* **1976**, *36*, 1072.

(33) Oxtoby, D. W. *Phys. Rev.* **1977**, *A15*, 1251.

(34) Hoye, J. S.; Stell, G. *J. Chem. Phys.* **1984**, *81*, 3200.

(35) Rzoska, S. J.; Chrapec, J.; Ziolo, J. *Physica* **1986**, *139A*, 569.

(36) Sliwiska-Bartkowiak, M. *Ber. Bunsenges. Phys. Chem.* **1990**, *94*, 64.

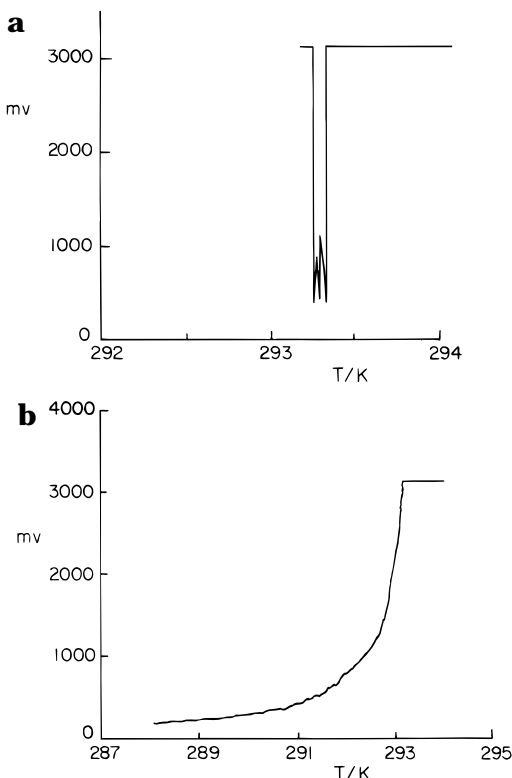


Figure 7. Photodiode voltage versus temperature for: (a) the bulk nitrobenzene (2)/*n*-hexane (1) mixture at the bulk critical composition, $x_2 = 0.42$; (b) the mixtures in Bio-Glas of 100 nm pore size, at the pore critical composition of $x_2 = 0.38$. In the case of the confined fluid, x_2 is the mole fraction in the coexisting bulk fluid.

thermostated with an accuracy of $\pm 2 \times 10^{-2}$ K, and the liquid temperature was measured by a copper–constantan thermocouple, with an accuracy of 5×10^{-3} K.

The liquids studied (nitrobenzene and hexane) were purified. The nitrobenzene was twice distilled under reduced pressure, dried over Al_2O_3 , and centrifuged prior to the measurement. The conductivity of the purified liquid was of the order of $10^{-9} \text{ W}^{-1} \text{ m}^{-1}$. The hexane was twice distilled and its conductivity was lower than $10^{-15} \text{ W}^{-1} \text{ m}^{-1}$.

The porous matrices consisted of Bio-Glas beads made by Bio-Rad (California), with a pore size of 100 nm. This material is composed of silica glass, contains no ions in the structure, and is chemically inert, except when subject to hydrofluoric acid and to solutions of pH above 10. The Bio-Glas beads had the following characteristics: porosity of 52% (fraction of bead volume occupied by internal pores); nominal void volume of 35% (the remaining volume is taken by the structure of the material); a material permittivity of $\epsilon_p = 1.025$; a high value of resistivity, $\sigma = 0.02$ nS. To remove air, the beads were kept under reduced pressure directly prior to the measurement.

5. Experimental Results

The liquid–liquid phase coexistence curve was determined for both bulk nitrobenzene–hexane mixtures and for mixtures confined in the controlled pore glass, using light transmission measurements. The photodiode voltage, proportional to the intensity of the light beam passing through the sample, was used as the measure of this intensity. In the case of the bulk mixture, for a given concentration, the phase transition temperature is indicated by a sharp decrease in the photodiode voltage, related to the strong turbidity of the system, as the temperature was decreased. An example is shown in Figure 7. As shown in Figure 7a, the temperature interval of the transition is very narrow, and the mixture separates into two separate liquid phases when the temperature decreases. By contrast, in the case of the mixture in Bio-Glas, the system remains turbid for temperatures lower

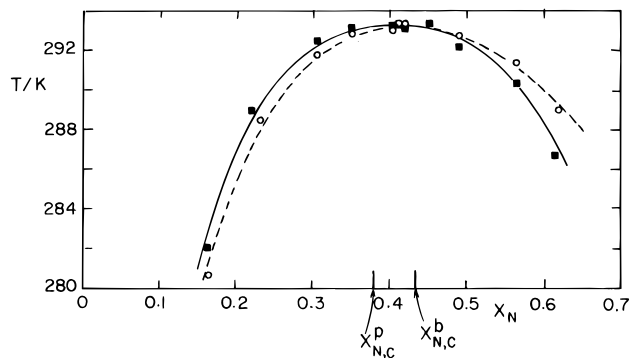


Figure 8. Liquid–liquid coexistence curves for nitrobenzene (2)/*n*-hexane (1) mixtures for the bulk mixture (○) and for the mixtures in Bio-Glas of 100 nm pore size (■); x_2 is the mole fraction in the (coexisting) bulk fluid.

than the temperature of phase separation (Figure 7b). The phase coexistence curves for both the bulk and confined mixtures are shown in Figure 8. The critical concentrations determined are $x_c^b = 0.42$ and $x_c^p = 0.38$ for the first and second cases, respectively. The corresponding critical temperatures are $T_c^b = 293.21 \pm 0.01$ K and $T_c^p = 293.16 \pm 0.01$ K. The phase coexistence curve of the nitrobenzene–hexane mixture on pores is shifted toward lower concentrations (the hexane-rich side) when compared to that obtained for the bulk mixture. This suggests that hexane is more attracted to the walls than nitrobenzene (see results of section 3). These shifts in the (apparent) critical composition and temperature are reasonable when considered in terms of the correlation length relative to the pore size, as discussed in the next section.

For the critical concentration of the bulk nitrobenzene–hexane mixture, the temperature dependence of the NDE has the typical power law character of eq 20, with critical exponent $\phi = 0.44 \pm 0.04$. This value is in line with values reported for ϕ for other mixtures, which range from 0.3 to 0.6; for many cases reported ϕ was about 0.4. Goulon et al.³⁷ using a droplet model of phase transitions, obtained the relation $\phi = \gamma - 2\beta \approx 0.59$, where γ and β are the usual critical exponents for the isothermal compressibility and density difference between the two phases, respectively; this relation was also obtained by Hoye and Stell³⁸ from an analysis of the statistical mechanics of a molecular liquid in an electric field. Using the usual scaling relations between critical exponents, ϕ can be related to more familiar critical exponents by

$$\phi = \gamma - 2\beta = (2 - \eta)\nu - 2\beta \quad (21)$$

where η and ν are the critical exponents for the total correlation function $h(r)$ and the correlation length ξ . The temperature dependence of the NDE for the bulk system is shown in Figure 9a; the NDE tends to infinity in the vicinity of the critical point, as expected. For the critical pore concentration of the mixture placed in Bio-Glas, the NDE remains finite as the apparent critical point is approached (Figure 9b). For the temperature range from 296 to 293.5 K, the curve approximately obeys eq 20 with a value of the critical exponent ϕ of 0.50 ± 0.05 . The change in the character of the NDE in the vicinity of the apparent critical temperature in the confined system is expected, because the correlation length ξ cannot grow greater than the pore diameter in the two dimensions normal to the pore axis. In such a situation we can expect the scaling behavior to change from Ising-like to classical

(37) Goulon, J.; Greffe, J. L.; Oxtoby, D. *J. Chem. Phys.* **1979**, *70*, 4742.

(38) Hoye, J. S.; Stell, G. *J. Chem. Phys.* **1984**, *81*, 3200.

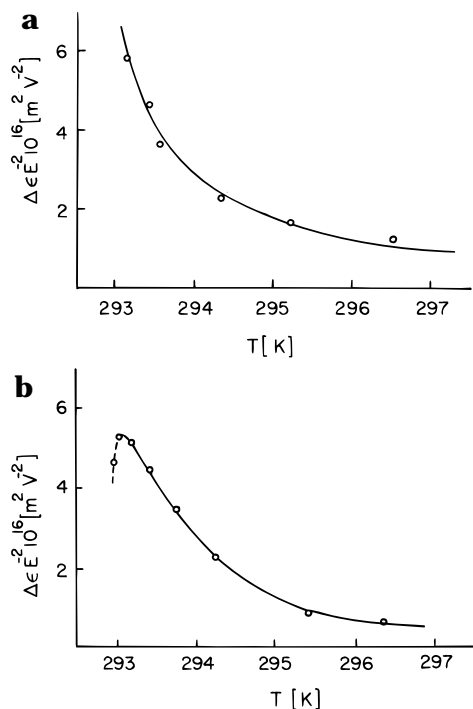


Figure 9. Temperature dependence of the NDE for: (a) the critical concentration x_2^p for the bulk nitrobenzene (2)/*n*-hexane (1) mixture; (b) the critical concentration x_2^p for the nitrobenzene/*n*-hexane mixture in Bio-Glas of 100 nm pore size.

when ξ approaches H .^{39,40} From eq 21 we expect ϕ to fall from about 0.5 to 0 in this region as the temperature is lowered from above the coexistence region, and the behavior shown in Figure 9b supports this expectation. It is possible that a discontinuity in the NDE occurs as the pore coexistence curve is crossed and the temperature enters the two-phase region, but this is not completely clear from the current data. The behavior shown in Figure 9b is also similar to that observed for mixtures with frozen critical fluctuations,^{41,42} in which, on lowering the temperature through the one phase region, the mixture freezes just before a consolute point would have been reached; in this case the growth of the correlation length is prevented by solidification. We note that the phenomenon shown in Figure 9b is not related to freezing of the mixture. We determined the freezing point of this mixture by the differential scanning calorimetry method, and found it to be $T_f = 268$ K.⁴³

We note that the apparent critical point in the controlled pore glass is not a true critical point; that is, the correlations can grow to infinity in only one dimension, along the axis of the pore, but such a growth in one dimension cannot produce a true critical point. Nevertheless, the behavior of the phase diagram resembles that of a bulk binary mixture, and we therefore refer to this as the apparent critical point in the pore.

6. Discussion and Conclusions

The density functional theory calculations show that in all cases studied the effect of confinement is to lower the critical mixing temperature and to reduce the range of

immiscibility, as observed by previous workers in simpler symmetric systems.^{8,9} When the fluid–wall attraction is greater for component 1 than for component 2, the coexistence curve is shifted toward the component 1-rich side of the diagram. The solubility of component 2 in the component 1-rich phase is thus reduced, while that of component 1 in the component 2-rich phase is increased; the changes in solubility are large, especially at the lower temperatures. Such changes will have important implications for the adsorption of trace components in soils and other porous media. These effects are enhanced when the pore size is reduced and when the difference in attractive fluid–wall forces for the two components is increased.

The experimental results for nitrobenzene/*n*-hexane mixtures in controlled pore glass with 100 nm pores are in qualitative agreement with these theoretical results. The liquid–liquid phase coexistence curve of the confined mixture is shifted toward the hexane-rich side of the diagram, suggesting that hexane is more strongly attracted to the walls than nitrobenzene. The critical concentration decreased by $\Delta x_2 = x_2^p - x_2^b = 0.04 \pm 0.01$, while the critical temperature was lowered slightly, $\Delta T_c = T_c^p - T_c^b = 0.05 \pm 0.02$.

That the observed lowering of the critical temperature due to confinement is reasonable can be seen from a consideration of the scaling law for the correlation length ξ , which is, in three dimensions

$$\xi = \xi_0 \left| \frac{\Delta T}{T_c} \right|^{-0.63} \quad \text{critical isochore} \quad (22)$$

where $\Delta T = T - T_c$ and ξ_0 has dimensions of the order of the molecular size and is usually in the range 0.1–0.3 nm⁴⁴ for most small molecules. If we assume $\xi_0 = 0.2$ nm and $T_c = 300$ K, eq 22 predicts that $\xi = 100$ nm when $\Delta T \approx 0.016$ K, which is of the order of the shift in critical temperature found experimentally.

In the bulk mixtures the correlation length and NDE both tend to infinity as the temperature tends to T_c at the critical composition. By contrast, for the mixture in the porous matrix the NDE tends to a finite value at the critical pore composition, an indication of the limitation placed on the increase in the correlation length due to pore size. In the case we have studied the pore size (100 nm) and maximum correlation length are comparable to the wavelength of light, leading to turbidity at the pore critical point. The behavior of the mixture in the controlled pore glass below T_c^p resembles that of a system with “frozen” critical fluctuations. This conclusion is supported by the strong turbidity that is observed far below T_c^p .

In future work we plan to study such confinement effects experimentally for smaller pores, where the effects will be more pronounced. Our theoretical and molecular simulation studies will also be extended to unsymmetrical mixtures with more realistic potentials in order to make direct comparisons with the experimental results.

Acknowledgment. It is a pleasure to thank J. Stecki and B. Widom for helpful discussions. We are grateful to the National Science Foundation (Grant CTS-9508680) and KBN (Grant 1450) for support of this research and also for support of our international cooperation through a Grant (INT-9511946) from the NSF/KBN cooperative research program.

LA960004A

(39) Mon, K. K.; Binder, K. *J. Chem. Phys.* **1992**, *96*, 6989.
 (40) Wilding, N. B.; Bruce, A. D. *J. Phys. Condens. Matter* **1992**, *4*, 3087. Bruce, A. D.; Wilding, N. B. *Phys. Rev. Lett.* **1992**, *68*, 193.
 (41) Sliwiska-Bartkowiak, M. *Phys. Lett.* **1988**, *128*, 84.
 (42) Sliwiska-Bartkowiak, M.; Szurkowski, B.; Hilczer, T. *High Temp.-High Pressures*, in press.
 (43) Gras, J.; Sliwiska-Bartkowiak, M. Manuscript in preparation.

(44) Sengers, J. V.; Levelt Sengers, J. M. H. *Annu. Rev. Phys. Chem.* **1986**, *37*, 189.